Journal of Applied Electrochemistry **31**: 193–199, 2001.

On minimum mass transfer at a sintered metal electrode

F. CŒURET
Laboratoire de Thermocinétique – UMR CNRS no 6607 – Nantes, implantation: Ecole Louis de Broglie, Campus de Ker-Lann, 35170 Bruz, France
(correspondence: e-mail: coeuret@isitem.univ-nantes.fr)

Received 15 February 2000; accepted in revised form 13 July 2000

Key words: minimum mass transfer, porous electrode, sintered metal electrode

Abstract

Limiting diffusion currents were measured at the inner surface of sintered nickel electrodes sheets and a model adapted from heterogeneous catalysis was used to quantify the minimum mass transfer within the porous material. External mass transport from the bulk electrolyte was induced by rotating a disc facing the sintered nickel disc electrode located at the bottom of a cylinder. Values of the volumetric mass transfer coefficient at two sintered materials were thus obtained. The method and its limitations are discussed.

List of symbols

a_e	specific surface area (m^{-1})
A_e	outer electrode surface area (m^2)
C_{AE}	concentration of A at the pore entrance (mol m^{-3})
C_{Ai}	concentration of A at the electrode surface (mol m^{-3})
$C_{A\infty}$	bulk concentration of A (mol m^{-3})
d_h	hydraulic diameter (m)
D_A	molecular diffusion coefficient (m^2 s^{-1})
D_A^*	apparent molecular diffusion coefficient (m^2 s^{-1})
e	thickness (m)
F	faradaic constant (96 487 C mol^{-1})
H	distance between the discs (m)
I	current (A)
I_L°	limiting diffusion current in the porous medium (A)
$(I_L)_t$	total limiting diffusion current (A)
$(I_L)_{ext}$	limiting diffusion current on A_e (A)
$(\overline{k_d})_{ext}$	outer mean mass transfer coefficient (m s^{-1})
$\overline{k_d^\circ}$	minimum mass transfer coefficient (m s^{-1})
l	width of a planar electrode (m)
L	length of a planar electrode (m)
N	speed of rotation (rpm)
p	slope (A m^3 mol^{-1} $(rpm)^{-1/2}$)
R_T	radius of the rotating disc (m)
Re_L	Reynolds number for boundary layer flow
Sc	Schmidt number
$\overline{Sh_{dh}^\circ}$	minimum Sherwood number based on D_A
$(\overline{Sh_{dh}^\circ})^*$	minimum Sherwood number based on D_A^*

Greek symbols

$\bar{\varepsilon}$	mean porosity
ε_i	superficial porosity
μ	dynamic viscosity (kg m^{-1} s^{-1})
ν	kinematic viscosity (m^2 s^{-1})
ν_e	number of electrons in the reaction (= 1)

1. Introduction

In a recent paper [1], the electrochemical method [2] was used to measure the minimum mass transfer coefficient between a stationary liquid and the inner surface of a sintered metal electrode. This quantity is useful to estimate the performance of a porous electrode whose pores contain a stationary electrolyte, and minimum solid to liquid heat transfer coefficients in the pores of a sintered material could be estimated by analogy. As pointed out in [1], other methods were used for minimum mass transfer measurements in fixed beds of grains. The aim of the present paper is to continue with the method presented in [1] and to analyse some of its characteristics.

2. Observations based on previous work

Figure 1 summarizes the method used in [1] for sintered nickel sheets and/or cylindrical walls. A sheet (thickness e, length L, width l) of sintered nickel was held parallel to a laminar uniform liquid flow (Figure 1(a)). Under such conditions, a viscous laminar boundary layer develops symmetrically on the two opposite faces. Similarly, symmetrical diffusional boundary layers

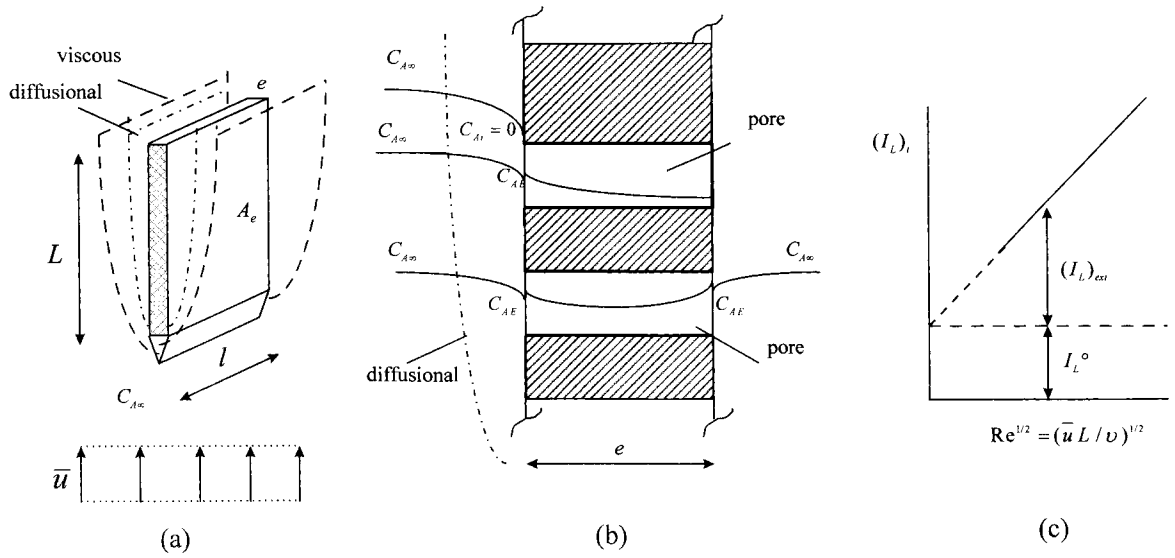

Fig. 1. Method used in [1, 5]: (a) sheet of sintered nickel, (b) models of pores and (c) mode of representation.

develop under limiting current conditions. The total limiting current $(I_L)_t$:

$$(I_L)_t = (I_L)_{ext} + I_L^\circ \tag{1}$$

is the sum of the limiting current at the outer surface $(I_L)_{ext}$, and the current at the inner surface of the sintered metal itself, I_L°.

Two straight cylindrical pores, as models of the porous medium, are shown in Figure 1(b): one is open at one extremity, the other one is open at both its extremities. The concentration of reactant A is distributed between the bulk liquid concentration $C_{A\infty}$ and the interior of the pore; at the pore entrance, the concentration is C_{AE}.

The minimum mean mass transfer coefficient, $\overline{k_d^\circ}$, or the mass transfer coefficient between the stationary electrolyte filling the pores and the pore wall, is calculated from I_L°. Such a current results from the competition between molecular diffusion of the reactive component A in the pores, and its electrochemical reaction at the pore wall, a problem which is analogous to that encountered in gas-solid catalysis with a first order irreversible chemical reaction. The developments based on this analogy were presented in [1]. For a pore open at one extremity, the following equation was obtained:

$$I_L^\circ = A_e v_e F (\overline{k_d^\circ} a_e D_A^*)^{1/2} C_{AE} \tanh\left\{ \left(\frac{\overline{k_d^\circ} a_e e^2}{4 D_A^*} \right)^{1/2} \right\} \tag{2}$$

which can be simplified to

$$I_L^\circ = A_e v_e F (\overline{k_d^\circ} a_e D_A^*)^{1/2} C_{AE} \tag{3}$$

when the argument of the hyperbolic function is higher than 3 [$\tanh(3) = 0.9951$]. When the pore is open at both extremities, Equations 2 and 3 again apply but with a supplementary multiplier of 2.

In the above equations, D_A^* is the apparent molecular diffusion coefficient of A in the continuous medium equivalent to the porous system of specific surface area a_e . It was shown by Oliveira Vilar [1, 5] that for sintered media of mean porosity $\bar{\varepsilon}$, D_A^* and D_A (true molecular diffusion coefficient) can be related as $D_A^*/D_A = (\bar{\varepsilon})^{1.7}$.

At the experimental conditions of Figure 1 $(I_L)_{ext}$ was proportional to $Re_L^{1/2}$ in agreement with boundary layer theory, and I_L° was obtained by extrapolating the straight line $(I_L)_t$ against $Re_L^{1/2}$, as shown in Figure 1(c).

The sintered cylindrical walls studied in [1] were also located as in Figure 1(a), but their pores were only accessible from one side. Minimum Sherwood numbers based on the hydraulic diameter d_h and the assumption of true molecular diffusion, $\overline{Sh_{dh}^\circ}$, or molecular diffusion in the equivalent continuous medium, $(\overline{Sh_{dh}^\circ})^*$, were calculated. The method was applied to fixed beds of grains or spherical particles, for the sake of testing and comparisons.

The application of the method to the system of Figure 1 suffers two shortcomings: (a) a uniform stationary isothermal laminar flow needs to be realized, with a variable mean velocity. Thus, the experimental set-up has to be a rather complex 'classical' laboratory hydraulic circuit including column, pump, rotameter, reservoir, bypass, tubes, valves, temperature control etc. Furthermore, the hydraulic system may generate vibrations which may affect the measurement of I_L°, and (b) for the application of Equations 2 and 3, C_{AE} has to be known. In [1] it was set constant and equal to $C_{A\infty} = 0.005$ M. Due to the fast electrochemical reaction, the concentration at the surface boundary (i.e., near the pore entrance) was zero ($C_{Ai} = 0$), hence this postulation is dubious.

A few comments about this point are in order. As in heterogeneous gas–solid catalysis, the global mass

transport between the bulk electrolyte and the sintered electrode results from two contributions in series: one is the external diffusional mass transport through the hydrodynamic boundary layer towards the pore opening, and the other is the diffusional mass transport within the pores with an electrochemical reaction at their walls . If C_{AE} is the same for all the pores, the equality of the two stationary transport fluxes yields:

$$(\overline{k_d})_{ext}(C_{A\infty} - C_{AE})\varepsilon_i A_e \equiv \frac{I_L^\circ}{v_e F} \quad (4)$$

where $(\overline{k_d})_{ext}$ is the external mean mass transfer coefficient and ε_i the fraction of A_e occupied by pore openings [due to the sintering of the material as sheets, ε_i is probably smaller than the mean porosity $\bar{\varepsilon}$]. Combining Equations 3 and 4 yields:

$$C_{AE} = \frac{\varepsilon_i(\overline{k_d})_{ext}}{\varepsilon_i(\overline{k_d})_{ext} + (\overline{k_d^\circ} a_e D_A^*)^{1/2}} C_{A\infty} \quad (5)$$

from which follow two limiting cases:

(i) $C_{AE} \approx C_{A\infty}$, when $\varepsilon_i(\overline{k_d})_{ext} \gg (\overline{k_d^\circ} a_e D_A^*)^{1/2}$, that is, when the internal mass transport process is controlling;

(ii) $C_{AE} \approx (\varepsilon_i(\overline{k_d})_{ext}/(\overline{k_d^\circ} a_e D_A^*)^{1/2})C_{A\infty}$, with the limit $C_{AE} \approx 0$, when the external mass transport is the controlling step. According to this limiting expression, C_{AE} varies with $(\overline{k_d})_{ext}$ and can be calculated only if $(\overline{k_d^\circ} a_e D_A^*)^{1/2}$ is known. For such an external mass transport control, Equation (3) becomes:

$$I_L^\circ = \varepsilon_i A_e v_e F(\overline{k_d})_{ext} C_{A\infty}$$

which means that the reaction current I_L° would be very small, originating from transport through the pore openings on A_e, and could not be distinguished from $(I_L)_{ext}$.

It thus follows that $\overline{k_d^\circ}$ can be obtained by this method only when $C_{AE} \approx C_{A\infty}$ i.e. when external mass transport is sufficient. If this external transport is not favoured, not only is C_{AE} smaller than $C_{A\infty}$ but it is not a linear function of $(\overline{k_d})_{ext}$. The same situation occurs for I_L° according to Equation 3. In such a case, the desirability of the method based on Equation 1 for the measurement of I_L° is not evident.

3. New application of the method

A device more simple than in [1] was used, mainly to experimentally investigate the influence of $C_{A\infty}$ in the application of the method. In order to produce a laminar hydrodynamic flow which could be varied easily, a cell previously used by Cavalcanti and Cœuret [6] for the study of mass transfer between a liquid and the bottom of a cylinder holding a rotating disc (Figure 2) was adapted. At laminar conditions, the mean mass transfer coefficient at the cylinder bottom (fixed disc) is directly proportional to the square root of the rotating disc velocity. Thus, if the fixed nickel disc of [6] is replaced by a disc of sintered nickel, the system allows a method similar to that of Figure 1(c) to be applied.

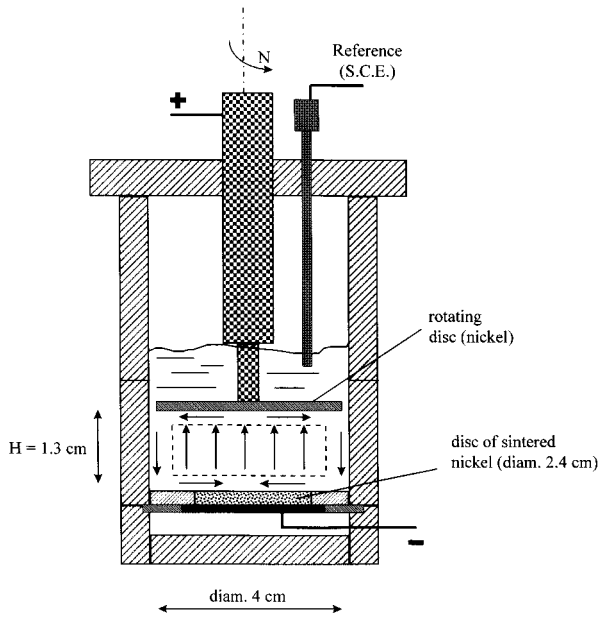

Fig. 2. View of the cell used in the present work.

In the lower part of the Altuglas cell, a nickel disc electrically connected with the exterior, was inserted. A circular disc of sintered nickel (dia. 2.4 cm) inserted in an annular PVC disc (dia. 4 cm) served as the bottom of the cylindrical cavity. The electrical connection to the disc of sintered nickel was made with a double flat spiral of nickel wire crossing a rubber disc acting as a gasket. Thus, the pores of the disc of sintered nickel were blocked at their lower extremity. The distance between the rotating and the fixed discs was $H = 1.3$ cm. As in previous experimental work [6, 7], the rotating disc (dia. 3.5 or 3.9 cm) was supported and driven by an adequately modified Tacussel-EDI rotating system.

Three types of sintered nickel sheets (SIKA Nx from Krebsoge, France) were used. Table 1 shows their characteristics: thickness, e, mean porosity, $\bar{\varepsilon}$, specific surface area per unit of total volume, a_e (obtained as in [1] from static pressure drop measurements); hydraulic pore diameter, d_h, and particle size before sintering (from the supplier catalogue). The letter x in SIKA Nx represents the filter grade (i.e., the size, in μm), of the smallest particle which can be held by the material if used as a filter.

The electrolyte was an aqueous solution of 0.5 M NaOH containing a mixture of 0.05 M $K_4Fe(CN)_6$ and $K_3Fe(CN)_6$ with $C_{A\infty} = 0.0025, 0.005, 0.0075, 0.01$ and

Table 1. Characteristics of materials

Sintered nickel	e /m	a_e /m^{-1}	$\bar{\varepsilon}$	d_h /μm	Particle diameter before sintering /μm
SIKA N2	0.0022	170,000	0.24	5	75–100
SIKA N10	0.0023	68,000	0.30	17	100–200
SIKA N20	0.00245	54,000	0.42	31	200–300

0.015 M. A fresh solution was prepared for each experiment. The porous disc was chemically activated with 50 wt % HCl , then rinsed with water, and its pores were filled with the solution just prepared; these operations were made by aspiration. The porous disc was installed into the cell in which about 70 ml of electrolyte were introduced. Before each experiment, the electrolyte was let stand for about one hour in order to reach equilibrium.

The disc of sintered nickel served as the cathode while the rotating disc was the anode. A reference electrode (SCE) was immersed from the top cover. The three electrodes (porous disc, full rotating disc, reference electrode) were incorporated into a three-electrode potentiostatic circuit including a Tacussel PRT-20 2X potentiostat associated with a Tacussel Pilovit–Num pilot unit. Since the cathode potential was changed linearly with time, the current–time curves are essentially equivalent to the current–potential curves. A small rotation velocity was fixed, and the cathodic potential was varied, thus generating a curve similar to that of Figure 3(a). In contrast to [1], there was no fluctuation in the current. As shown in Figure 3(a), each curve represents a decrease corresponding to the establishment of the stationary concentration profile within the porous cathode. $(I_L)_t$ is the limit of the registered current. Before choosing another rotation velocity, time was again allotted to the system to reach equilibrium. The experiments were made at 20 °C. The value of the molecular diffusion coefficient of ferricyanide at 20 °C, $D_A = 6.96 \times 10^{-10}$ m^2 s^{-1}, was calculated from the Stokes–Einstein expression established in [1] from many determinations.

4. Results and discussion

Figure 3(b) shows, for SIKA N10 and $C_{A\infty} = 0.01$ M, the variations of $(I_L)_t$ with $N^{1/2}$. Extrapolation to $N = 0$ leads to I_L°. Figure 4 summarizes the direct results obtained for SIKA N10 and SIKA N20 and different bulk concentrations. Figure 3(b) demonstrates the $I_L^\circ(A_e v_e F D_A^{*1/2})$ group as a function of $C_{A\infty}$ to be the test of the applicability of Equation 3. Figure 5 provides results obtained with the three materials used.

Several remarks follow from the analysis of this Figure: (i) For SIKA N10, since linearity is not obtained for $C_{A\infty} < 0.0075$ M, the condition $C_{AE} \approx C_{A\infty}$ might be possible only for sufficiently high values of $C_{A\infty}$. At $C_{A\infty} = 0.0025$ M, the value $I_L^\circ = 0$ implies that $C_{AE} \approx C_{Ai} = 0$. The plot corresponding to SIKA N20 is linear, perhaps because the pores of this material are larger than those of SIKA N10. Reproducibility was obtained only for two concentrations in the case of SIKA N2 (see Figure 5); as a consequence, the results were not further analysed. In [1] where SIKA N2 was

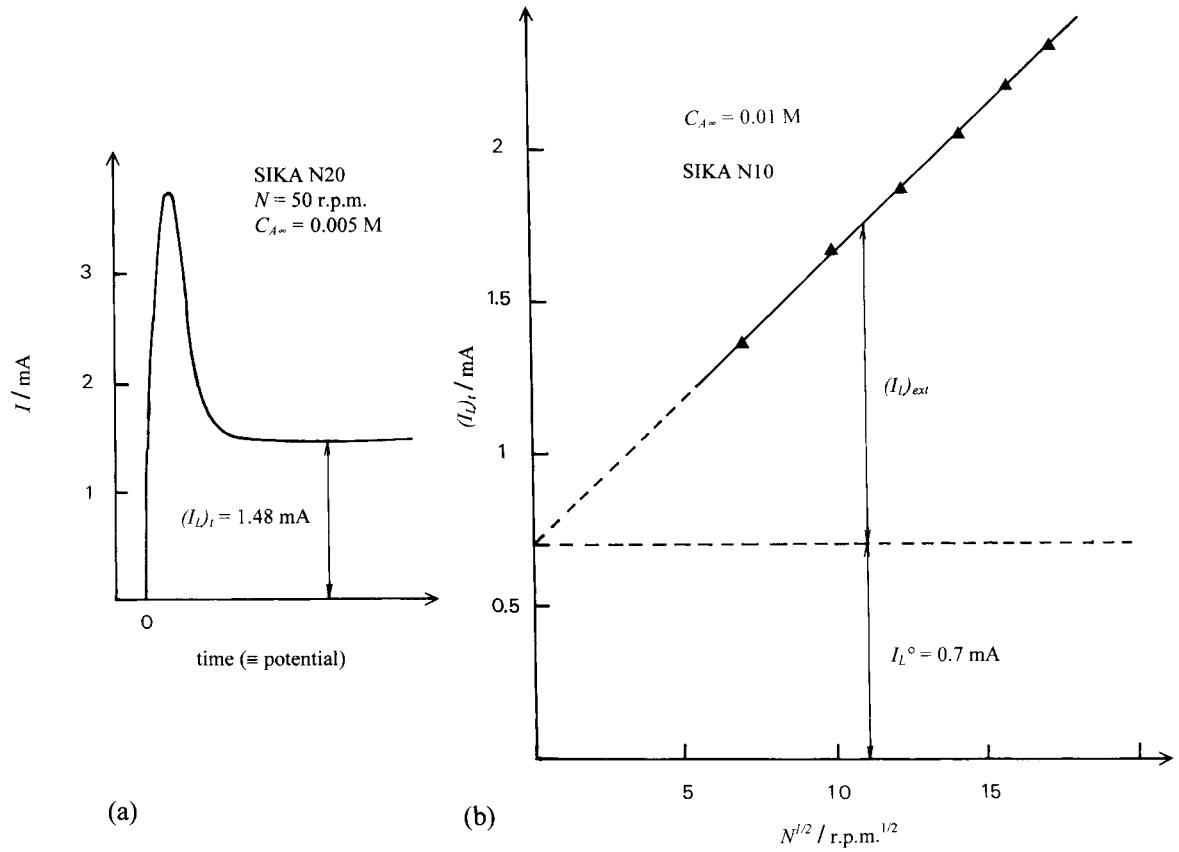

Fig. 3. Examples of results: (a) current–time (potential) curve and (b) variations of $(I_L)_t$ with $N^{1/2}$.

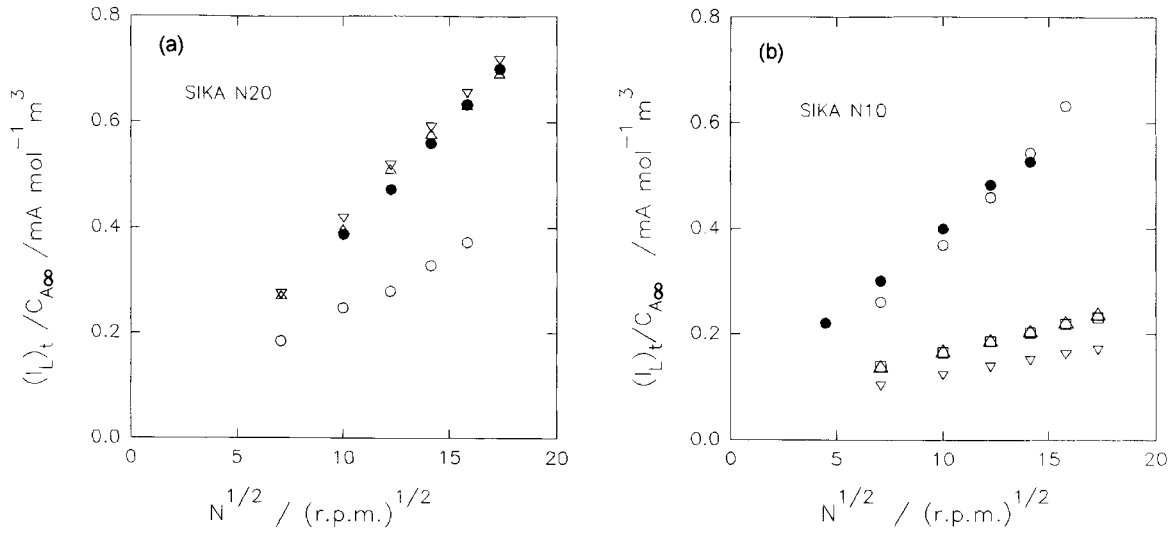

Fig. 4. Global results obtained for SIKA N10 and SIKA N20. Key: (○) 0.025, (▽) 0.005, (▲) 0.0075, (△) 0.01 and (●) 0.015 M.

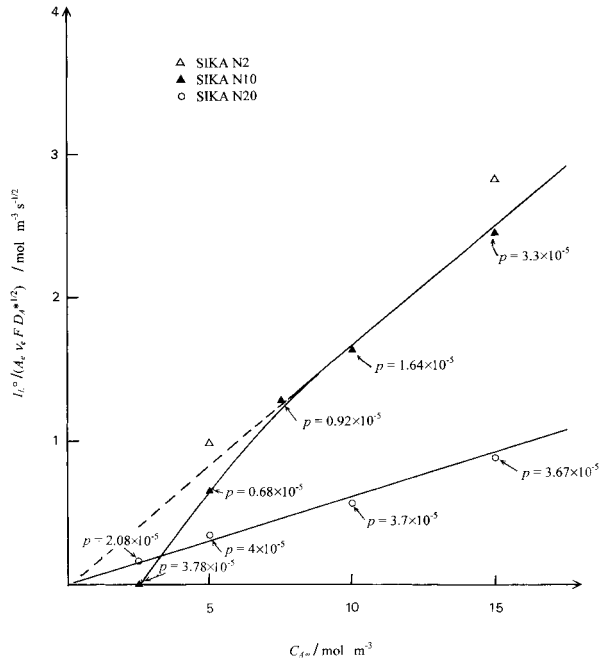

Fig. 5. Variations of $I_L^\circ/(A_e v_e F D_A^{*1/2})$ with $C_{A\infty}$.

used as in Figure 1(a), difficulties were also encountered, although the pores were open at their two extremities.

(ii) Equation 3 allows calculation of $\overline{k_d^\circ} a_e$ from the slope of straight lines of plots such as Figure 4. In [1], the current $(I_L)_{ext}$ was compared, with reasonable satisfaction, to the value calculated from the application of boundary layer theory for mass transfer. In the present case, $(I_L)_{ext}$ was compared to the current corresponding to mass transfer at a fixed disc below a rotating disc of radius R_T in a cylinder, under similar conditions of size and confinement. The calculation of this current was made from the following empirical correlation:

$$\frac{(\overline{k_d})_{ext} H}{D_A} = 0.2\left(\frac{H}{R_T}\right)^{-0.28}\left(\frac{2\pi N H^2}{60\nu}\right)^{1/2} Sc^{1/3} \qquad (6)$$

established in [6] with a fixed disc defining the bottom of the cylindrical cavity, and valid for the present experimental conditions where $H/R_T = 0.65$ and $940 < 2\pi N H^2/(60\nu) < 5650$. According to Equation 6, the $(I_L)_{ext}/C_{A\infty}$ ratio should vary with $N^{1/2}$ and Figure 4 is in agreement with this prediction, if the constancy of $I_L^\circ/C_{A\infty}$ is admissible in the domain of variation of $C_{A\infty}$. Applied to the present case (fixed disc, dia. 4 cm), the slope calculated from Equation 6 would be $p = (I_L)_{ext}/(C_{A\infty} N^{1/2}) \approx 10^{-5}$ A m^3 mol^{-1} (rpm)$^{-1/2}$.

It is interesting to investigate how the slope p, deduced from the experiments with the sintered electrodes varies with $C_{A\infty}$. In a rigorous application of the method, p would be a constant for a given material. If not, an erroneous value of I_L° would be obtained from plots such as Figure 3(b), in spite of the linearity of $(I_L)_t$ against $N^{1/2}$ (Figure 4). The value of p corresponding to every experimental point of Figure 5 is indicated (materials SIKA N10 and SIKA N20) and Figure 6 is finally obtained. For a given material, p first decreases when $C_{A\infty}$ is increased from small values. It then reaches a minimum and increases up to a limiting value approximately equal to that corresponding to the values of $C_{A\infty}$ near zero. The existence of such a limit at high values of $C_{A\infty}$ is clear for SIKA N20 but not in the case of SIKA N10. This indicates (in the case of SIKA N20) that beyond a given value of $C_{A\infty}$, mass transfer at the outer surface of the sintered metal is well quantified by $(I_L)_{ext}/C_{A\infty}$, and that the contribution of I_L° to $(I_L)_t$ corresponds well to mass transfer within the porous material.

The fact that p is not a constant regardless of $C_{A\infty}$ for a given material means that $C_{AE} < C_{A\infty}$ and that it varies with $C_{A\infty}$, as indicated by Equation 5. As a consequence, setting $I_L^\circ/C_{A\infty}$ = constant leads to the underestimation of the contribution of the porous medium to the total current. According to the model leading to Equation 5, the minimum observed in Figure 5 would suggest that external mass transport is

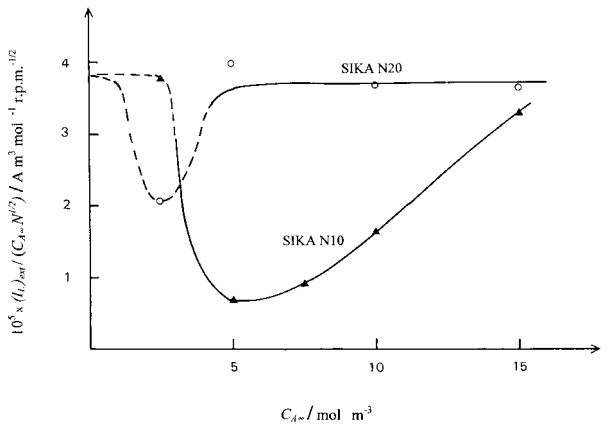

Fig. 6. Variations of with $(I_L)_{ext}/(C_{A\infty}N^{1/2})$ with $C_{A\infty}$.

not very strong compared with internal transport. Calculations of $(\overline{k_d})_{ext}$ from Equation 6 yield $4.1\times 10^{-6}\,m\,s^{-1}$ for $N = 50$ rpm and to $1.0\times10^{-5}\,m\,s^{-1}$ for $N = 300$ rpm while the minimum values of $(\overline{k_d^\circ}a_e D_A^*)^{1/2}$ deduced from I_L°, assuming $C_{AE} = C_{A\infty}$, are $8\times10^{-7}\,m\,s^{-1}$ for SIKA N20 and $1.5\times10^{-6}\,m\,s^{-1}$ for SIKA 10. Thus $(\overline{k_d})_{ext}$ can be considered much larger than $(\overline{k_d^\circ}a_e D_A^*)^{1/2}$ only for SIKA N20.

The minima in Figure 6 can also be explained by the difference in size between the pore openings and the hydrodynamic laminar boundary layer thickness. The mean spatial value of the latter calculated from Equation 6 is 17 μm for $N = 50$ rpm and 4 μm for $N = 300$ rpm; these values are somewhat smaller than the hydraulic diameter of SIKA N10 and SIKA N20, respectively (Table 1). This could explain why, even if $(I_L)_{ext}$ is proportional to $N^{1/2}$, a sufficiently high bulk concentration $C_{A\infty}$ is necessary to reach a concentration value C_{AE} which is not influenced by the zero surface concentration ($C_{Ai} = 0$) existing on A_e all around the pore openings. Material SIKA N2 is not adequate for the application of the method, due to its very small pores and high specific surface area.

For SIKA N20, the limiting value of p is $\approx 3.7\times10^{-5}\,A\,m^3\,mol^{-1}\,(rpm)^{-1/2}$ (Figure 6); except its order of magnitude, this value cannot be compared with that ($\approx 10^{-5}\,A\,m^3\,mol^{-1}(rpm)^{-1/2}$) calculated from Equation 6. Indeed, as shown in [6], the radial distribution of the local mass transfer coefficients on the fixed disc is not uniform, in as much as the local coefficient decreases from the axis to the periphery. The 2.4 cm diameter sintered nickel disc is smaller than the 4 cm diameter cylindrical cavity to which Equation 6 applies, thus justifying the difference between the calculated and the observed values of p.

As a consequence of Figure 6, the method of obtaining $\overline{k_d^\circ}$ from electrochemical measurements which allows a distinction between $(I_L)_{ext}$ and I_L° appears to be strictly applicable in the present case only for SIKA N20 and for $C_{A\infty} \geqslant 0.005$ M. Figure 6 shows that $C_{A\infty} \geqslant 0.015$ M must be maintained for SIKA N10.

Assuming that $C_{AE} = C_{A\infty}$, the values of $\overline{k_d^\circ}a_e$ (volumetric minimum mass transfer coefficient) determined from the application of the method are:

(i) for SIKA N10: $\overline{k_d^\circ}a_e = 0.028\,s^{-1}$. According to Figure 5, such a value would be underestimated. However it agrees with the value $0.02\,s^{-1}$ obtained by OliveiraVilar and Cœuret [1] using the technique of Figure 1(a).

(ii) for SIKA N20: $\overline{k_d^\circ}a_e = 0.0037\,s^{-1}$, a value which agrees with those deduced in [1, 5] for fixed beds of microspheres. With such a value of $\overline{k_d^\circ}\,a_e$, the argument of the hyperbolic function of Equation 2 would be equal to 6, thus justifying the a posteriori simplification of Equation 2 to Equation 3.

Obviously, the method given in [1], and considered again in the present paper, is only appropriate when $(I_L)_{ext}$ is not much higher than I_L°, in order to make the application of Equation 1 possible. This not only implies the use of small rotating velocities of the disc, but it also restricts the method to porous materials possessing a sufficiently high total surface area, independently of their specific surface area.

These clarifications of material in [1] allow improvements in using the model. In spite of limitations, the method shows that the known [8] analogy between heterogeneous catalysis and porous electrodes can be applied to the acquisition of experimental data useful for the design of porous electrodes. The importance of $\overline{k_d^\circ}a_e$ in the design of porous electrodes with stationary electrolyte must be recognized for the extension and possible improvements of the method given in [1].

5. Conclusions

The method first used in [1] to measure the minimum mass transfer rate to the inner surface of a sintered electrode, was applied to a simpler experimental cell. It is shown that the concentration at the pore entrance is an important variable. When the bulk electrolyte concentration is not sufficiently high, the method underestimates the reaction current corresponding to the porous medium, and hence the numerical value of the minimum mass transfer coefficient.

The known analogy between heterogeneous catalysis and the behaviour of porous electrodes offers a new field of research aiming for a better design of porous electrodes with stationary electrolyte. However, further investigations may well be warranted because of the limitations of the method.

References

1. E. Oliveira Vilar and F. Cœuret, *Can. J. Chem. Eng.* **77** (5) (1999) 855–862.
2. J.R. Selman and C.W. Tobias, 'Mass transfer measurements by the limiting current technique', *Advances in Chemical Engineering*, Vol. 10 (Academic Press, New York, 1978), pp. 211–318.

3. T. Miyauchi, *J. Chem. Eng. Japan* **5** (1972) 303–305.
4. T. Miyauchi, T. Kikuchi and K. Hsu, *Chem. Eng. Sci.* **31** (1976) 493–498.
5. E. Oliveira Vilar, 'Transfert de Matière entre un Fritté Métallique et un Liquide: Application aux Electrodes Poreuses Percolées', Thesis (University of Rennes 1, Rennes, France, 1996).
6. E.B. Cavalcanti and F. Cœuret, *J. Appl. Electrochem.* **26** (1996) 655–663.
7. S. Langlois, J.O. Nanzer and F. Cœuret, *J. Appl. Electrochem.* **19** (1989) 736–743.
8. F. Cœuret, D. Hutin and A. Gaunand, *J. Appl. Electrochem.* **6** (1976) 417.